Vol. 479: 263–282, 2013
doi: 10.3354/meps10189

MARINE ECOLOGY PROGRESS SERIES
Mar Ecol Prog Ser

Published April 8

Tidal and subtidal currents affect deep aggregations of right whale prey, *Calanus* spp., along a shelf-basin margin

Kimberley T. A. Davies*, Tetjana Ross, Christopher T. Taggart

Department of Oceanography, Dalhousie University, 1355 Oxford Street, Halifax, Nova Scotia B3H4R2, Canada

ABSTRACT: North Atlantic right whales *Eubalaena glacialis* foraging on deep (>100 m) populations of diapausing *Calanus* spp. in the Roseway Basin right whale Critical Habitat (south of Nova Scotia, Canada) are most often located along the southern margin of the basin. We investigated the physical and biological oceanographic characteristics that make this margin a lucrative feeding ground. Bottom-moored acoustic Doppler current profilers equipped with conductivity, temperature, and depth sensors were deployed cross-isobath on the southeastern slope of the basin to simultaneously measure variation in *Calanus* spp. concentration, current velocity, and water mass characteristics in time and space. Variation in upslope tidal advection of deep-basin water with densities >1026 kg m^{-3} and containing highly concentrated copepod aggregations was the most important process influencing cross-isobath variation in copepod concentrations on the slope. The aggregations were maintained in the slope region through time despite extensive along-isobath advection, implying the existence of copepod re-supply mechanisms to the southern margin. Proposed mechanisms include immigration from surface populations, horizontal advection, and gyre-like re-circulation within the basin. A simple empirically-driven particle tracking model illustrated tidally-forced particle convergence between the 100 and 140 m isobaths on the southeastern slope, followed by upward and along-isobath advection. Cross-isobath 'compression' of copepods coupled with the maintenance of their vertical position through neutral buoyancy is proposed as a mechanism resulting in accumulation on the slope, making the area uniquely beneficial to right whales feeding at depth along the slope margin.

KEY WORDS: *Calanus* · Water mass density · Acoustic Doppler current profiler · Tides · Roseway Basin · Right whale · Sloped margin

INTRODUCTION

North Atlantic right whales *Eubalaena glacialis* are highly endangered large cetaceans that face significant mortality from fishing gear entanglement and vessel strikes (Kraus & Rolland 2007). Efforts to reduce these threats continue to improve through Canadian and international legislation implemented as recently as 2008 that protects their feeding and breeding habitats (e.g. Vanderlaan & Taggart 2009, Vanderlaan et al. 2011). Conservation strategies are employed based on the best available habitat data; however, our understanding of what constitutes right whale habitat is in some respects quite poor (Baumgartner et al. 2003). In particular, physical and biological mechanisms that create and maintain large aggregations of the primary right whale food source, *Calanus finmarchicus* stage C5, are not characterized for most habitats. Diagnostic assessment of these mechanisms requires simultaneous collection of data — in time and space (i.e. a Lagrangian frame of reference) — on water mass circulation, hydrography, and food abundance in relation to the whales, a tractable task for only the most focused interdisciplinary sampling programs.

*Email: kim.davies@dal.ca

Grand Manan Basin in the Bay of Fundy (Canada) is a right whale feeding habitat where, through the combined effort of many research programs, significant progress has been made in describing the mechanisms that maintain *Calanus* aggregations (e.g. Woodley & Gaskin 1996, Laurinolli 2002, Baumgartner et al. 2003, Michaud & Taggart 2007, 2011, Aretxabaleta et al. 2008). Together, these and other studies have found that the planktonic food is advected by tidal currents in the basin that accumulate and maintain patches of C5 copepods at depths >100 m to the benefit of foraging whales. Strong tidal currents advect C5s along the ~8 km tidal excursion (Michaud & Taggart 2011), and right whales have been observed to move with the tide, presumably to maximize consumption of the advecting patches of food (Laurinolli 2002, Baumgartner et al. 2003). Patch integrity appears to be maintained at tidal cycle scales and likely at weekly scales or more (Michaud & Taggart 2011). Annual maxima in right whale sightings in the basin correspond with the timing of maximum C5 abundance at depth (Michaud & Taggart 2007) and also the maximum particle retention due to a seasonal gyre in the basin that is partially maintained by tidal rectification (Aretxabaleta et al. 2008). Further, the historical right whale sighting probability distribution in Grand Manan Basin is elliptical and oriented parallel to the cross-isobath tidal ellipse, with the distribution center located near the geographic center of the basin (Fig. 1b,d). This is strong evidence that advection by tidal currents consistently affects the distribution of whales and, by inference, their food on inter-annual time scales (Michaud & Taggart 2011). The maintenance of a

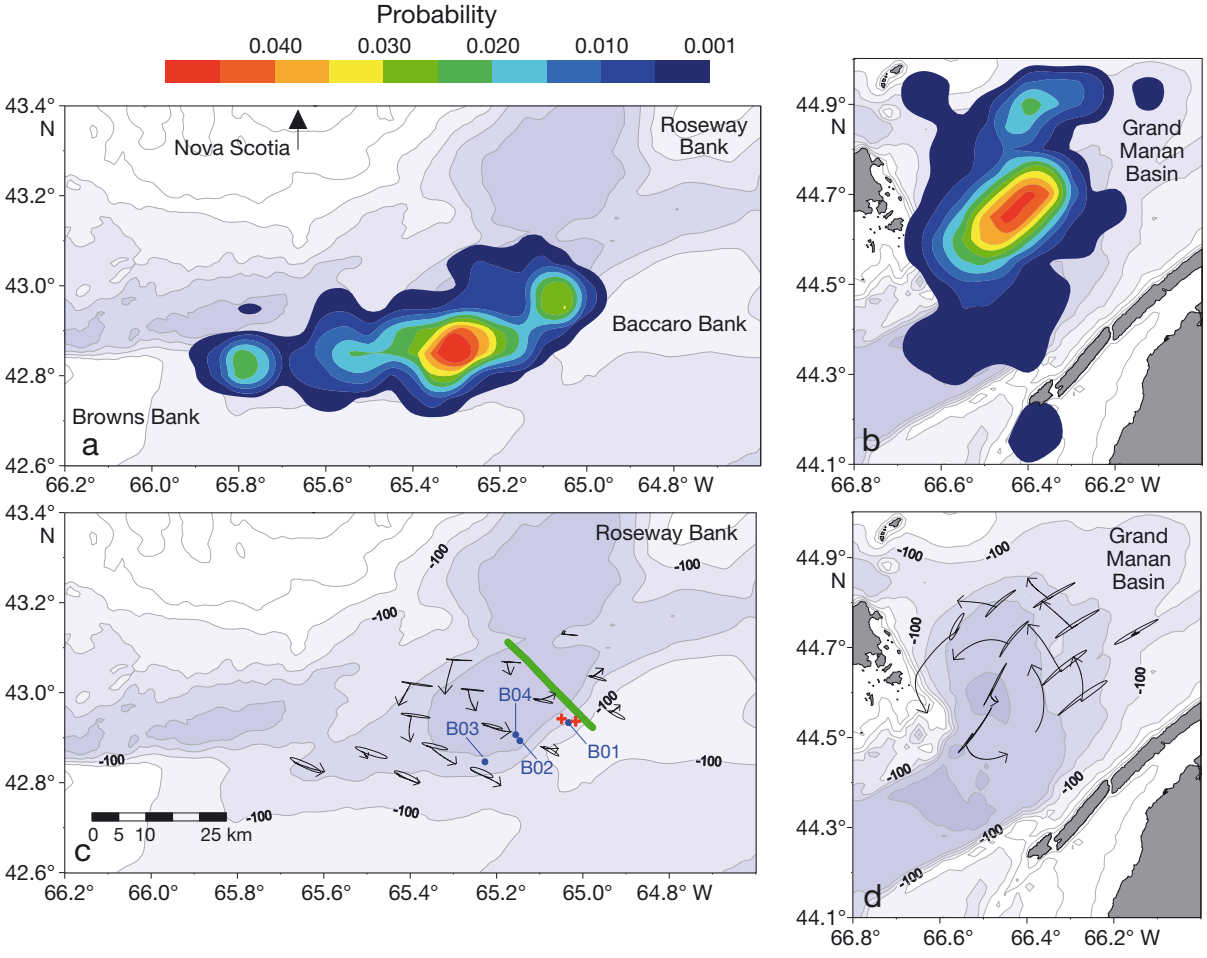

Fig. 1. *Eubalaena glacialis.* Bathymetric (25, 50, 75, 100, 125, 150, 200 m isobaths) charts illustrating the probability distribution of right whales occupying (a) Roseway Basin and (b) Grand Manan Basin (after Vanderlaan et al. 2008), and (c,d), modeled circulation at 100 m depth for mid-September 2008 in each basin, respectively, based on WebDrogue v. 0.66 (Ocean Science Division, Bedford Institute of Oceanography), where line-arrows illustrate 60 h displacement and direction forced by the M2 subtidal flow, and ellipses illustrate the M2 tidal ellipses. Also illustrated in (c) are locations of ADCP and CTD moorings (red crosses), biological net-collections (blue circles with identifier labels), and the CTD profiling section (green line)

dense, high-energy food source by persistent and predictable tidal processes in Grand Manan Basin offers a simple explanation as to why approximately one-third of all North Atlantic right whales return to the habitat to forage for ~3 mo each year.

The right whale population is loosely divided according to habitat fidelity into those that repeatedly habituate the Bay of Fundy and those that do not (Schaeff et al. 1993). Many of the non-Fundy whales feed during late summer in nearby Roseway Basin on the western Scotian Shelf (Baumgartner et al. 2003, Vanderlaan et al. 2008). Roseway Basin, like Grand Manan, maintains diapausing *Calanus finmarchicus* C5 aggregations that are also co-located with the less abundant diapausing *C. hyperboreus* C4 copepodites (Davies et al. 2012), each with enhanced energy content and apparently maintaining neutral buoyancy at the depths (>100 m) where they rest. Based on the findings in Grand Manan Basin, it is reasonable to speculate that oceanographic conditions in Roseway Basin also serve to accumulate and maintain the food resources commensurate to the metabolic needs of right whales and other plankton predators that habituate Roseway. However, the processes influencing the prey field in Roseway may differ from Grand Manan because the water masses, tides, currents, and bathymetry — all factors that affect the prey field in Grand Manan — differ between the 2 habitats.

An observer in Roseway Basin has the highest probability of sighting a right whale along the southern margins of the basin between the 100 and 160 m isobaths (Vanderlaan et al. 2008; Fig. 1a). A general circulation model shows that, like Grand Manan Basin, the southern margin of Roseway has tidal ellipses oriented normal to the isobaths, and a weak along-isobath subtidal flow (Webdrogue ver. 0.66; Ocean Science Division, Bedford Institute of Oceanography; Hannah et al. 2001; Fig. 1b,d). The right whale sighting distribution in Roseway Basin is oriented differently with respect to the tidal ellipse and bathymetry than in Grand Manan Basin. This prompted us to investigate the oceanographic processes that could explain differences in the sighting distributions of right whales between the 2 habitats. Our study was based on 2 major questions: (1) Why is the long axis of the right whale sighting distribution in Roseway oriented along-isobath and roughly normal to the tidal ellipse (Fig 1a,c), whereas in Grand Manan Basin, the long axis of the sighting distribution is oriented cross-isobath and parallel to the tidal ellipse? We hypothesized that because the tidal currents are much weaker in Roseway than in Grand Manan (Fig. 1c,d), the along-isobath mean flow may be the dominant forcing mechanism affecting the distribution of the whale food and hence the whales in Roseway. (2) Why is the sighting distribution of right whales in Roseway centered along the slope of the southern basin margins, whereas in Grand Manan Basin, the center of the sighting distribution is located over the geographic center of the basin? Given the spatial and tidal coincidence of the concentrated prey field and the whales in Grand Manan (Michaud & Taggart 2011), the whale distribution in Roseway would suggest that the southern slope margin of Roseway is the most favorable feeding ground. While we had little information concerning the distribution of diapausing copepods (C4s and C5s) in Roseway, those in the nearby LaHave and Emerald Basins to the east are highest in abundance at depth (>200 m) in the basin centers where current velocities are small (Herman et al. 1991). Right whales, however, do not regularly exploit the potential habitats in the Lahave or Emerald Basins, leading us to hypothesize that the biological and physical oceanographic characteristics that make the southern slope-margin of Roseway a lucrative feeding ground may be unique to this basin.

Physical mechanisms associated with a tidal front on a slope, detailed below, may be responsible for the maintenance of C4 and C5 aggregations at depth along the southern margin of Roseway. Patches of diapausing copepods can accumulate through the interaction between current velocity and the maintenance of vertical position by the animals (Franks 1992). In Grand Manan Basin, C5s were 3-fold more abundant in warm, salty, deep water on the basin side of a tidal front that defined the inshore basin margin, than they were in the cold and fresh Bay of Fundy water mass on the inshore side of the front (Michaud & Taggart 2011). The latter authors hypothesized that the front could act as a barrier to the inshore advection of C5s, and proposed that upslope mixing of the neutrally dense C5s during flood tide, and their subsequent sinking during ebb tide at the front edge, could maintain the aggregation in the deep waters of the basin. Consistent with this hypothesis, Lagrangian particle velocity estimates on the northern and southern slopes of Georges Bank suggested a cell pattern, with particles at depth and on-bank being advected toward the surface and particles in the upper water column being advected off-bank and downward (Wishner et al. 2006).

Critical to these hypotheses is an understanding of the process by which C5s use buoyancy to maintain their vertical position while diapausing at depth. It is

generally assumed that, to minimize use of stored lipid-energy during diapause, the animals maintain their vertical position passively in a density layer where they are neutrally buoyant. Tests of this hypothesis are limited to a few diagnostic modeling studies (e.g. Visser & Jonasdottir 1999, Campbell & Dower 2003, Campbell 2008) because diapause has yet to be induced in the laboratory. These above studies found that lipids play an important role in the buoyancy properties of the animals, but neutral buoyancy at depth cannot be achieved passively using lipids alone, partly because lipids have different thermal and pressure compressibility than seawater (Campbell & Dower 2003). To maintain neutral buoyancy, there must be active regulation by the animal, for example through regulation of internal ionic composition (Sartoris et al. 2010). Diagnostic buoyancy models have not been developed for shelf-basin overwintering populations of C5s, and this remains a knowledge gap (Campbell 2008). Hence the process of depth maintenance by diapausing copepods has not been fully characterized, and the assumption of passive neutral buoyancy may not be valid, but it is a useful first approximation.

Our contemporary conception of the circulation within Roseway Basin derives from a broad-scale seasonal-mean circulation model (Hannah et al. 2001) and current meter data from nearby Browns Bank (Smith 1989). While these sources are valuable for generating hypotheses, few data have been collected in the basin with the appropriate resolution required to address our questions. Therefore, we investigated the influence of tidal and subtidal currents on the right whale prey-field in Roseway Basin using moored acoustic Doppler current profilers (ADCPs) deployed across the southeastern slope of the basin during the September period of annual maximum right whale occupancy. This is the first time the basin has been outfitted with ADCPs, and we used them, along with other sampling and monitoring gear, to (1) investigate variation in C4 and C5 concentration at high resolution and at the scale of the foraging whales (i.e. metres to kilometers), and (2) assess the predictions of circulation models and test the hypotheses we developed regarding right whales and their food that are based on the assessments.

MATERIALS AND METHODS

Field survey

Two Workhorse Sentinel ADCPs (RD Instruments) equipped with 4 upward-looking transducers and pressure and temperature sensors were deployed in Roseway Basin during the period 4 through 13 September 2008 (day of year 248–257; hereafter "Day") from the RV 'Dominion Victory' (Table 1). Each RDI was housed in a streamlined underwater buoyancy system (SUBS; Open Seas Instrumentation) unit suspended 15 m above the seafloor, anchored by a train wheel, and recovered following a remotely-controlled acoustic release. Each SUBS unit was fitted with an internally recording Seabird-37 MicroCat conductivity, temperature, depth (CTD) sensor and a 3-transducer downward-looking 1-MHz Nortek ADCP (Aquadopp). The Aquadopps were used in concert with the Workhorses to collect full water column profiles of acoustic backscatter and current velocity, with the exception of a 4 m blanking region at the SUBS depth (±2 m). Mooring and ADCP-specific frequencies, location, bottom depth, and deployment period are provided in Table 1. The ADCPs recorded data using 1 m vertical bins and 2 min ensemble intervals with 150 pings per ensemble. The CTDs recorded data every 20 s, and the data were subsequently averaged over 2 min bins. Moorings were separated by approximately 1 tidal excursion (2.7 km) normal to the southeastern slope of the basin to measure cross-isobath current variation, acoustic backscatter, pressure, temperature, and salinity at a location where right whales have a high probability of being observed (Fig. 1c).

Zooplankton samples were collected using a multiple opening-closing net system (BIONESS; Sameoto et al. 1980) to provide zooplankton samples for

Table 1. Summary of each instrumented mooring deployed over day of year 248 through 257 (2008) on the southern margin of Roseway Basin including location, bottom depth, upward-looking 'Workhorse' acoustic Doppler current profiler (ADCP) frequency, and attached downward-looking Aquadopp ADCP frequencies and conductivity, temperature, depth sensors (CTD)

Mooring	Deployment period	Location (lat., long.)	Bottom depth (m)	ADCP frequency (kHz)	Other instruments
Shallow slope	249–257 (8 d)	42.9363° N, 65.0167° W	112	600	1MHz Aquadopp, Seabird-37 CTD
Deep slope	248–257 (9 d)	42.9419° N, 65.0495° W	134	300	1MHz Aquadopp, Seabird-37 CTD

ground-truthing ADCP acoustic backscatter. BIONESS was deployed at 4 locations (B01–B04) along the southern margin during the ADCP deployment period (Fig. 1c) and was equipped with 7 nets (333 µm mesh), either a Seabird-19 CTD or Seabird-37 CTD, pitch sensors, 2 digital flow meters (General Oceanics), and an optical particle counter (OPC; Herman 1988, 1992). Time of day and position of each tow is provided in Table S1 in the Supplement (www.int-res.com/articles/suppl/m479p263_supp.pdf). Casts at stations B01 and B04 began with an oblique net-tow to ~10 m above bottom, and the remaining nets were opened consecutively every 5 min until the surface was reached. At station B02, all but 1 net were used to sequentially sample the same depth (~131 m), and station B03 was a depth-integrated tow only. Samples were stored in 4% buffered formalin and processed in the lab where all zooplankton were subsampled, identified, and counted. BIONESS-net zooplankton concentrations were estimated following the methods detailed by Michaud & Taggart (2011).

A cross-section of the hydrography across Roseway Basin, normal to the southern slope, was measured on Day 253 (9 September) using a Endeco® V-fin fitted with a MicroCat CTD, an OPC (as above) and a G.O. digital flow meter, and was towed in an undulating (tow-yo) manner between 50 m depth and ~10 m above bottom using a vertical speed of ~1 m s^{-1} and ship speed of ~5.5 km h^{-1} along a pre-determined transect that passed near to the ADCP locations (Fig. 1c). Technical problems with the digital flow meter resulted in our approximating location and speed through the water using GPS vessel-location data and associated speed-over-ground along with the change in CTD depth. Sectional-profiles of water column properties were contoured using Surfer (Ver. 8, Golden Software) with interpolation based on inverse square distance, search ellipse radii of ~10 m vertical and ~3 km horizontal.

Relative zooplankton concentration estimation

The ADCP transducers were not calibrated and thus provided relative volume-scattering strength (Sv), and hence, only relative zooplankton concentration estimates (s, number of dominant scatterers m^{-3}, and $S = 10 \times \log_{10}(s)$) for each ADCP. This relative zooplankton concentration estimate is obtained from $S = Sv - TS$, where Sv is computed following Deines (1999), and TS is the average target strength of the dominant scatterer. Details concerning the estimation of s are provided in the Supplement (www.int-res.com/articles/suppl/m479p263_supp.pdf) along with echograms of S (dB) (Fig. S1).

The depth-structured BIONESS-net data indicated that diapausing copepods were concentrated in a 30 m thick layer at ~100 m depth (Tables S2 to S5 in the Supplement). The acoustic backscatter showed that the zooplankton were most concentrated in the 90 to 130 m depth layer at the deep-slope mooring and in the 80 to 110 m depth layer at the shallow-slope mooring (Fig. S1). Subsequently, for each mooring and at each time step, we depth-averaged $s(z,t)$ and the horizontal current velocities over the zooplankton layers defined above (ignoring the blanking region at the SUBS depth), and divided each value of the resulting time series $s(t)$ and the original matrix $s(z,t)$ by the minimum value of the time series; i.e.

$$s_{rel}(t) = s(t) / \min(s(t)) \text{ and } s_{rel}(z,t) = s(z,t) / \min(s(t)) \quad (1)$$

to provide an easily interpretable variable showing the changes in relative concentration over time. The s_{rel} term represents a unitless scaling factor with respect to the minimum concentration in the series; e.g. a value of $s_{rel}(t) = 10$ is 10-fold greater than the layer-averaged minimum concentration measured over the deployment period. An attempt was made to use co-located BIONESS and OPC data to estimate the 'real' minimum concentration and to convert s_{rel} into absolute concentration. However, we opted to use s_{rel} because the absolute concentration is very sensitive to error in the minimum concentrations estimated by the BIONESS (net estimates) and OPC (optical estimates).

RESULTS

Hydrography

The interior of Roseway Basin contained warm, salty water (10 to 15 km mark, Fig. 2a,b) similar in temperature and salinity (T-S) to continental slope water on the southern bank of the basin. Colder and fresher continental shelf water was evident at shallow depths across the basin, and its influence deepened to ~80 m toward the northern (shoreward) margin of the basin (left side, Fig. 2), causing a cross-basin tilting of isohalines ≤32.8. Across the southern slope region adjacent to the shoaling bank (right side, Fig. 2), the water was slightly colder and fresher than either mid-basin (10 to 15 km mark, Fig. 2) or southern bank (26 km mark, Fig. 2) water, indicative of mixing between cold, fresh continental shelf water and warm, salty slope water. A tidal-mixing front was

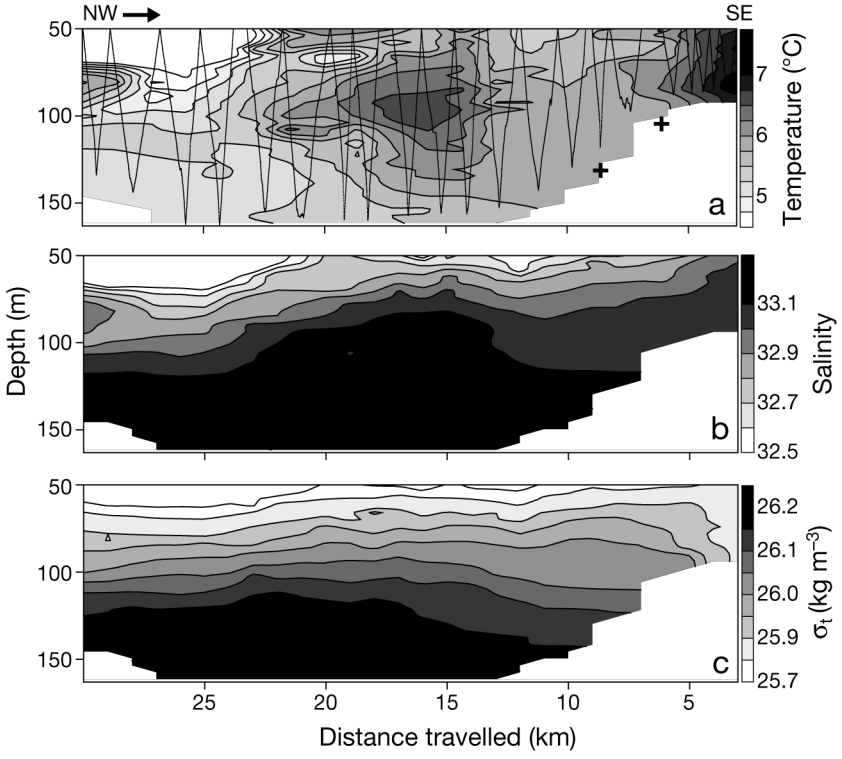

Fig. 2. Isopleth representations of (a) temperature (°C), (b) salinity, and (c) density (σ_t, kg m^{-3}) across a ~27 km CTD section (see Fig. 1), 50 m depth to ~10 m above the seafloor (white space), from the NW to SE margins (directional arrow) of Roseway Basin on Day 253 (9 September 2008) where the CTD profile (solid zigzag line) and approximate locations of the shallow and deep-slope ADCP moorings (black crosses) are provided in (a)

evident on the southern slope near the shallow ADCP mooring (distance >5 km and between 50 and 100 m depth, Fig. 2a,c), where near the 100 m isobath the distribution of isotherms and isopycnals changed from generally vertical to generally horizontal, indicating a change from stratified conditions in the basin to mixed conditions on the bank. The mid-basin continental slope water was surrounded by fresher shelf and shelf-slope mixed-water causing a characteristic 'doming' of the isohalines and isopycnals at depth that is typical of shelf basins.

At the ADCP moorings, water mass temperature, salinity, and density varied tidally and across a front that moved over the ADCPs during the first half of the series. Density and salinity varied by ~0.3 units over the time series, while temperature varied by 3°C (Fig. 3). Both temperature and salinity contributed to the density variation, but at different times one or the other was the larger contributor. Water density at depth varied at a semi-diurnal tidal scale and had a negative trend throughout the first half of the

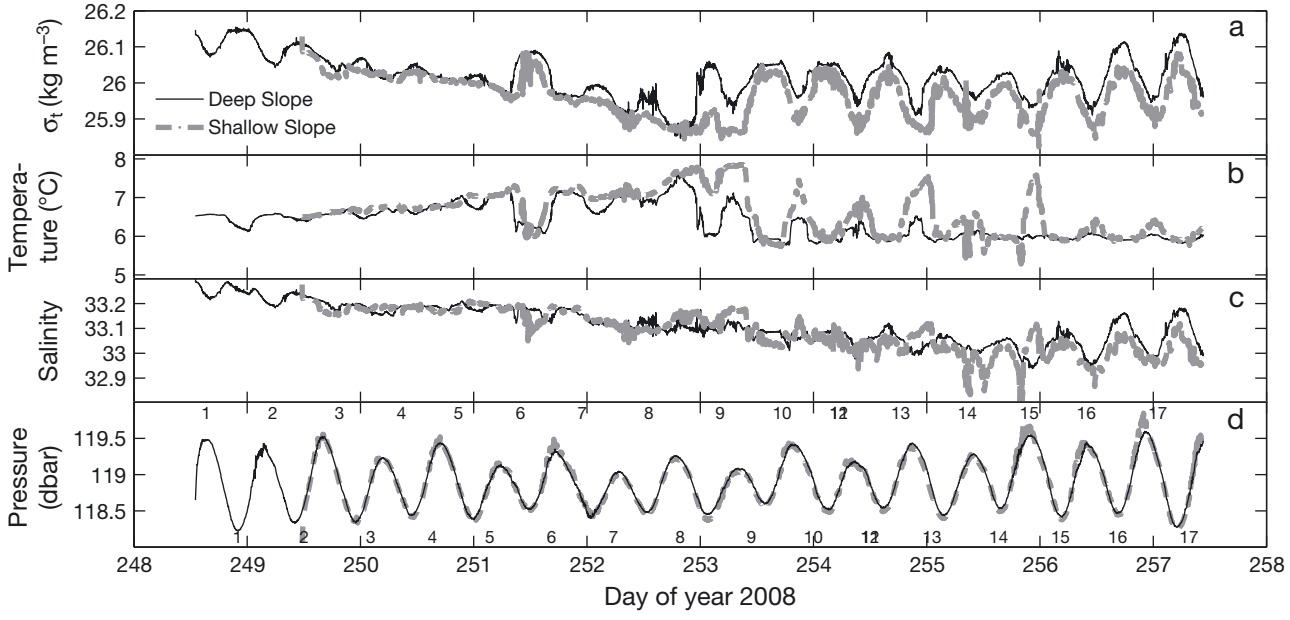

Fig. 3. Time series of (a) density, (b) temperature, (c) salinity, and (d) Aquadopp ADCP pressure at the shallow-slope (dashed grey line, offset +22 dbar for comparison) and deep-slope (solid black line) moorings on the southern slope of Roseway Basin during Days 248 through 257, 2008. Tide sequence numbers (1–17) in (d) are referred to in the Results

series (Fig. 3a). Density decreased during ebb tide and increased during flood tide, consistent with tidal variation expected for a cross-isobath density gradient on a slope. The M2 tidal variation and subtidal variation were separated using harmonic analysis (Matlab®: t_tide; Pawlowicz et al. 2002). The subtidal variation during the first half of the series was best described by a linear decrease before Day 253 at each mooring; $\sigma_t = 37.5 - 0.0459\ t(day)$ at the deep mooring and $\sigma_t = 39 - 0.0518\ t(day)$ at the shallow mooring ($r^2 = 0.76$ and 0.81, respectively, $p < 0.001$). Thereafter, the density variation was tidally dominated and exhibited no subtidal variation for the remainder of the 9 d deployment period. During the declining phase, the semi-diurnal density variation was damped across some tidal periods. Change in density associated with low tides 1, 2, and 6 were similar in amplitude to those of the second half of the series, while changes associated with low tides 3–5, 7, and 8 had reduced amplitude. This pattern was observed at both moorings, although dampening was greater at the shallow mooring. Density was most similar between moorings when the tidal signal was most damped (i.e. the cross-isobath density gradient decreased), suggesting that the same water mass was observed at both moorings during those times.

When temperature, salinity, and density variation through time at each mooring were examined within and between each series using T-S diagrams, we were able to identify at least 3 water masses on the southeastern slope of Roseway Basin during the deployment period. During the first half of the series, the T-S signature illustrated a mixture between colder (~5.8°C) and saltier (~33.25) water from the deep basin that had greater influence at low tide (water mass 1, Fig. 4), and warmer (~7.8°C), fresher (~33.15) water from upslope that had greater influence at high tide (water mass 2, Fig. 4). Water mass variation between high and low tide was roughly cross-isopycnal, except during the 'replacement period' addressed below, this section. As time progressed toward the middle of the series, the influence of water mass 1 declined and the influence of water mass 2 increased, causing water temperature at both moorings to increase steadily from ~6.2 to ~7.5°C while salinity and density decreased.

During the period of Day 252 to 253, there was a relatively abrupt change in the water mass characteristics at both moorings, as water mass 2 began to be replaced by a colder (~6°C), fresher (~32.95) water mass (water mass 3, Fig. 4). Water mass 3 was similar in temperature but fresher than water mass 1. Replacement by water mass 3 began at the deep-slope

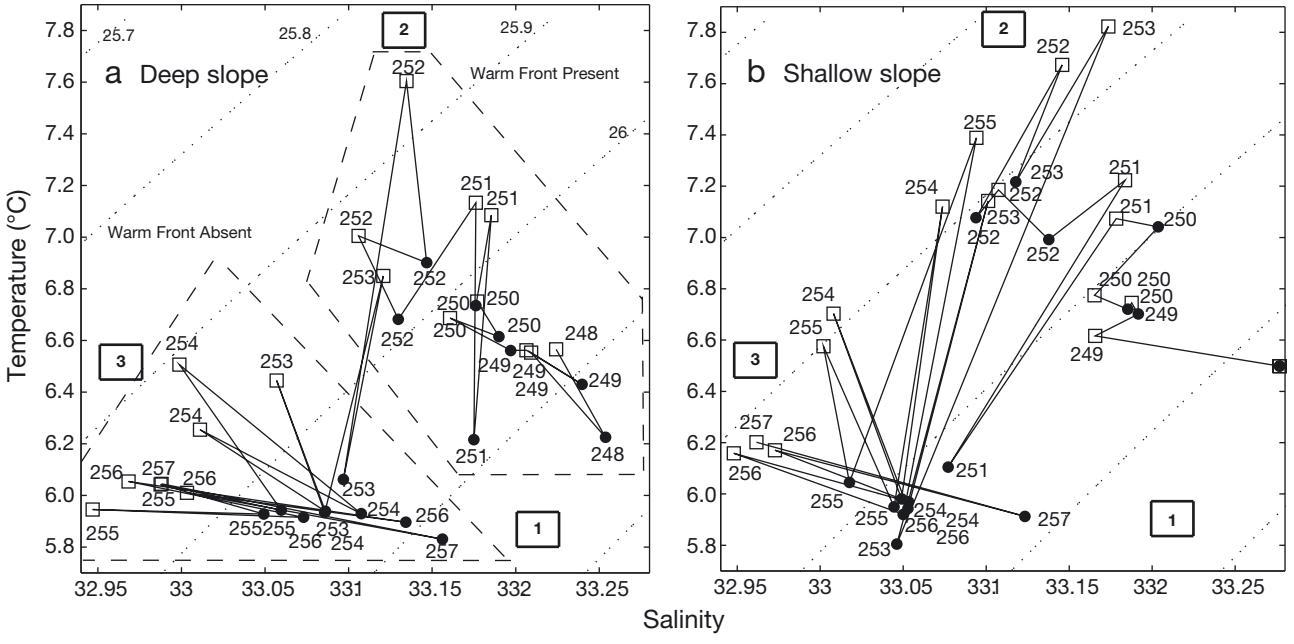

Fig. 4. Temperature and salinity (T-S) diagrams, derived from the CTD time series data collected at the (a) deep- and (b) shallow-slope moorings in Roseway Basin, where each datum represents the T-S state observed at each semi-diurnal high (small open squares) and low tide (closed circles) on Days 248 through 257, 2008 (labeled), and where solid lines join the tidal sequence. The dotted lines represent the σ_t isopycnals with magnitudes provided in (a). Water mass identity (1, 2, 3, large open squares) end-members referred to in the Results are labeled, and periods when the warm front associated with the advection of water mass 2 was present or absent are encompassed by a dashed-line polygon

mooring, and within 1 tidal cycle, water mass 2 disappeared from the T-S signature during low tide on Day 253. Water mass 2 subsequently disappeared at the shallow mooring during low tide 1 tidal cycle later. At both moorings, water mass 2 disappeared less quickly from the upslope water observed at high tide. Water mass 2 was completely replaced by water mass 3 at the deep-slope mooring by Day 254 and at the shallow mooring by Day 256. These changes in hydrographic properties were a basin-wide phenomenon; a small change in temperature was measured mid-basin using a sensor deployed at ~150 m depth (data not shown). With the water mass replacement and the absence of the front, variation in T-S and density became predominantly tidal (Fig. 3) and followed the consistent, cross-isopycnal gradient created by the mixing line between the end-member water masses 1 and 3 (Fig. 4). As opposed to the replacement period, the above tidal gradient was salinity driven with very little change in temperature, as apparent in Fig. 3b,c where the temperature signal gradually dampened at the end of the series, while the salinity signal was amplified.

Velocity and inferred displacement

Tidal variation in velocity was dominated by the M2 tide, with the long axis of the tidal ellipse being ~3 km and oriented cross-isobath at both moorings (deep: 2.76 km, 320° True; shallow: 3.36 km, 316.5° True; Matlab®: t_tide; Pawlowicz et al. 2002). Eighty-five percent of the variance in tidal velocity at the deep mooring was explained by the M2 and M4 constituents with amplitudes 0.20 and 0.01 m s^{-1}, respectively. Similarly, 86.6% of the variance in tidal velocity at the shallow mooring was explained by the same 2 constituents with amplitudes 0.24 and 0.02 m s^{-1}, respectively. To separate the effects of tidal velocities and subtidal velocities (i.e. residual velocities after removal of tides, hereafter 'subtidal flow'), the horizontal current velocity was decomposed into along-isobath (+$V(z,t)$, toward the northeast), and cross-isobath (+$U(z,t)$, upslope) directions. As there were no significant tidal contributions to $V(z,t)$, we assumed that the majority of variation in $V(z,t)$ was due to subtidal flow. $U(z,t)$ contained both tidal $U_{tide}(z,t)$ and subtidal (period >3 d, $U_{sub}(z,t)$) variation. We separated $U(z,t)$ into $U_{tide}(z,t)$ and $U_{sub}(z,t)$ using the tidal parameters provided from harmonic analysis (Matlab®: t_tide; Pawlowicz et al. 2002). The total 2D subtidal flow $sub(z,t)$ is the sum of the subtidal flows in the along-isobath $V(z,t)$ and cross-isobath $U_{sub}(z,t)$ directions.

We primarily used velocity in the form of the cumulative displacement (i.e. the time integral) of both the depth-specific $V(z,t)$ and $U(z,t)$, where

$$d_A(z,t) = \sum_{t'=1}^{t} A(z,t') \quad (2)$$

and layer-averaged $V(t)$ and $U(t)$, where

$$d_A(t) = \sum_{t'=1}^{t} A(t') \quad (3)$$

and $A = V$ or U. To clarify terminology used for the remainder of the paper, d_U and d_V are the displacements in the cross- and along-isobath directions, respectively. All of the variation in d_V is subtidal, and d_U is divided into tidal ($d_{U_{tide}}$) and subtidal ($d_{U_{sub}}$) variation. d_{tide} is the total tidal displacement, where $d_{tide} = d_{U_{tide}} + d_{V_{tide}}$ (and $d_{V_{tide}} = 0$), and d_{sub} is the total sub-tidal displacement, where $d_{sub} = d_{U_{sub}} + d_V$. This displacement representation makes it easier to identify patterns in the subtidal flow than does the velocity representation because changes in the residual are small at short time scales relative to the amplitude of the tidal changes. Velocities are provided in Figs. S6 & S7 in the Supplement.

At the deep mooring, layer-averaged $U(t)$ varied between 15 and 29 cm s^{-1} among tidal cycles at maximum ebb (upslope) and between 14 and 35 cm s^{-1} at maximum flood (downslope). Layer-averaged velocity was greater at the shallow mooring by ~4 cm s^{-1} in both the upslope and downslope directions, where it varied between 16 and 38 cm s^{-1} at maximum ebb and 13 and 41 cm s^{-1} at the maximum flood. The layer-averaged tidal excursion, represented by $d_{tide}(t)$, was highly variable among tidal cycles, ranging from ~1 to 6 km and partially dependent on the spring–neap cycle; neap tide occurred on Day 252 (Fig. 5).

During the first half of the deployment, the subtidal flow was moving primarily northeast along-isobath, and was dominated by $d_V(t)$ at both moorings (Fig. 6). A much smaller cross-isobath component displaced water downslope into the basin with greater displacement at the shallow mooring than at the deep mooring; i.e. there was a cross-isobath gradient in $d_{U_{sub}}(t)$. Despite this gradient, there was no difference in the displacement per day between the shallow mooring and the deep mooring (paired t-test, $p = 0.110$) because the influence of $d_{U_{sub}}(t)$ was small relative to $d_V(t)$ (Fig. 6). The subtidal flow was on average 10 cm s^{-1} (range 10 to 35 cm s^{-1}), and displaced 10 to 15 km of water per day over the ADCP moorings during the first 4 d. Displacement began to slow at the deep mooring on Day 253 and at the shallow mooring on Day 254. As the subtidal flow slowed, it turned downslope and into the basin, i.e. $d_{U_{sub}}(t)$ became

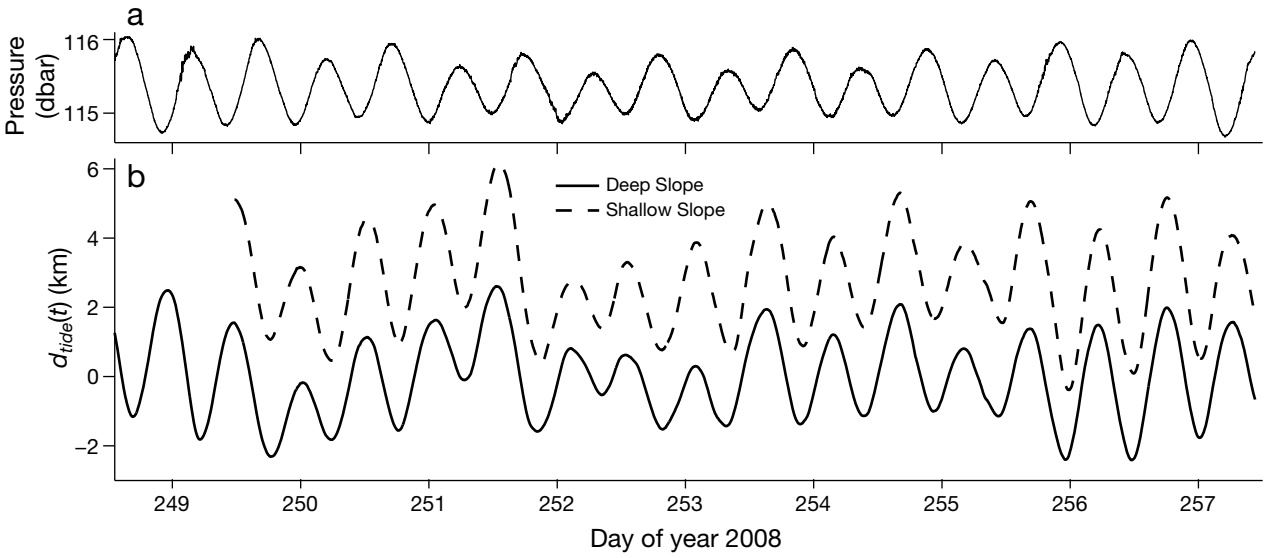

Fig. 5. Water pressure time series (a) at the deep-slope mooring and (b) the layer-averaged cumulative displacement of the tide, $d_{tide}(t)$, at the deep- (solid line) and shallow-slope (dashed line) moorings in Roseway Basin during Days 248 through 257, 2008, where the $d_{tide}(t)$ ordinate is labeled with respect to the deep-slope mooring and where the estimates for the shallow-slope mooring, located 2.7 km upslope from the deep-slope mooring, are offset +2.7 km relative to the deep-slope mooring estimates for comparison

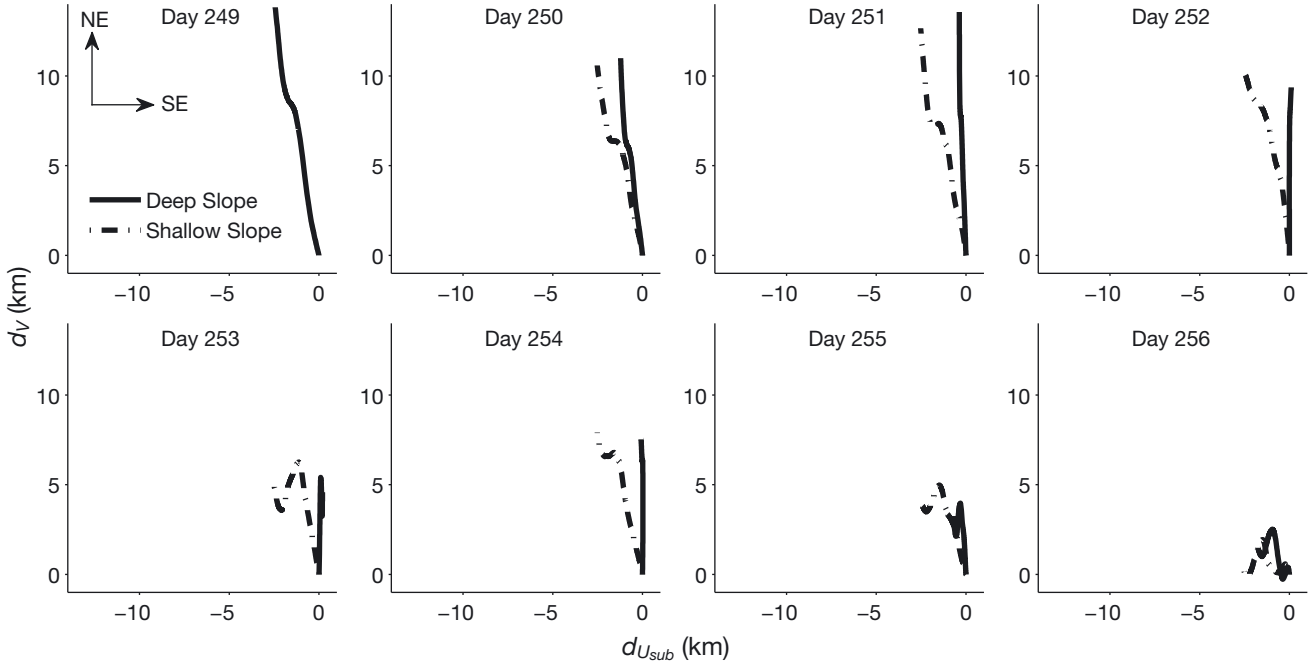

Fig. 6. Eight day sequence of 24 h layer-averaged cumulative-displacement estimates for the subtidal velocities, $d_V(t)$ and $d_{U_{sub}}(t)$, measured at the deep- (solid line) and shallow-slope (dot-dash line) ADCP moorings in Roseway Basin where the displacement vectors are oriented in relation to the southern basin margin (Fig. 1) with + $d_{U_{sub}}$ upslope (across-isobath) to the southeast on the abscissa and +$d_V(t)$ along-slope (along-isobath) to the northeast on the ordinate

dominant at both moorings and a small tidal component in the along-isobath direction became evident (Fig. 6).

The above results concern the layer-averaged bulk displacement, but the depth-specific $d_V(z,t)$ and $d_U(z,t)$ components each illustrated displacement variation within the zooplankton layer as well (Fig. 7). The magnitude of $sub(z,t)$, illustrated by the total 2D subtidal variation in the $d_V(z,t)$ and $d_U(z,t)$ components for each mooring location (Fig. 7) was smallest

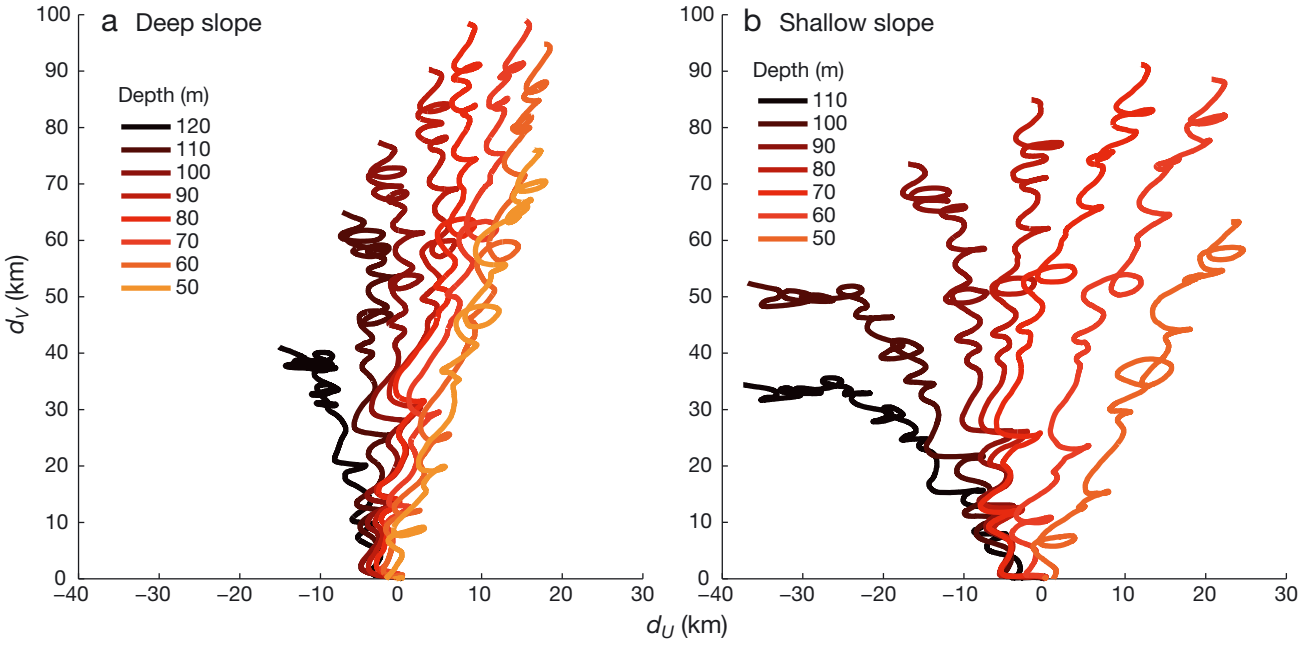

Fig. 7. Colour-coded (lines) of depth-specific (50 to 120 m at 10 m depth increments) cumulative displacement estimates over the 9 d deployment period in Roseway Basin in the along-isobath, $d_V(z,t)$, and cross-isobath $d_U(z,t)$, directions at (a) the deep- and (b) shallow-slope moorings. Displacement vectors are oriented in relation to the southern basin margin (Fig. 1) with + $d_U(z,t)$ upslope (across-isobath) to the southeast on the abscissa and +$d_V(z,t)$ along-slope (along-isobath) to the northeast on the ordinate

near-bottom and increased with decreasing depth to a maximum at ~70 m depth, then began decreasing again at ~60 m depth. In addition to changes in magnitude, the subtidal flow also changed direction from downslope near the seafloor ($-d_{Usub}(z,t)$) to along-isobath at ~80 m ($d_{Usub}(80,t) = 0$), and to upslope above 80 m ($+d_{Usub}(z,t)$); consistent with changes expected in a bottom Ekman layer. The change in direction, indicated by the magnitude of $d_{Usub}(z,t)$, was more pronounced at the shallow-slope mooring than at the deep-slope mooring. We estimated the bottom Ekman layer thickness (h_{WM}) for a stratified flow at the deep- and shallow-slope moorings during maximum ebb (upslope) and maximum flood (downslope) tides following Taylor & Sarkar (2008). At the shallow mooring, we estimated h_{WM} to be 55 m at maximum ebb tide, and 102 m at maximum flood. At the deep mooring, h_{WM} was about half as large; 25 m at the maximum ebb tide, and 55 m at maximum flood tide. Near-bottom (120 m at the deep slope, and 100 to 110 m at the shallow slope) and near the end of the series ($d_V(z,t) \cong 40$ km at the deep slope and 30 to 50 km at the shallow slope) $d_V(z,t)$ virtually stopped, while the magnitude of $d_{Usub}(z,t)$ remained relatively constant. This resulted in a strong downslope displacement at the shallow mooring, and almost no downslope displacement at the deep mooring, consistent with the cross-isobath gradient in $d_{Usub}(z,t)$ observed during the remainder of the series (Fig. 7). The vertical velocities were unreliable, and the details are provided in the Supplement (see 'Problems estimating the vertical velocities').

The subtidal flow appears to have been generated, at least partially, by density-driven geostrophic flow and Coriolis rectification. As a first approximation, the contribution due to density-driven flow was calculated using the thermal wind equations (see Eq. S2 in the Supplement) and the sectional density data (Fig. 2); an example calculation is provided in the Supplement. The density structure indicated a velocity of 2 to 4 cm s^{-1} amounting to approximately ~1/3 of the total subtidal flow. In Coriolis rectification, an along-isobath subtidal flow current is generated by nonlinear tidal advection when there is a cross-isobath velocity gradient over a sloping bathymetry (Loder 1980). The southern slope region of the basin has the necessary characteristics to generate rectified flow. These include a sloping bathymetry and a cross-isobath tidal ellipse (Fig. 1) and a cross-isobath tidal velocity gradient (Fig. 5). Our ADCP series is too short to definitively identify Coriolis rectification as a mechanism generating subtidal flow. Assuming rectification was occurring, a first approximation of the rectified subtidal flow was estimated to be ~3 cm s^{-1} (B. Petrie pers. comm.).

Plankton layer source and cross-slope width

The zooplankton layer originated downslope in the basin and was pushed upslope on the southeastern margin only during low tide (Fig. 8). The relative zooplankton concentration estimates, s_{rel}, increased at both moorings when the tide began to ebb, first at the deep mooring and shortly thereafter at the shallow mooring. The concentrations reached maxima during low tide at both moorings and then decreased, first at the shallow mooring and later at the deep mooring. During high tide, and throughout the series, s_{rel} remained consistently near the series minimum.

Although plankton concentrations increased with every ebb tide, the magnitude of the increase differed strongly among tidal cycles at both moorings. Below, we focus on the deep mooring only, although the trends were similar at the shallow mooring. During the first half of the series, concentrations remained relatively low at low tide except during tides 2 and 6 where concentrations were 322- and 360-fold higher than the series minimum, respectively (Fig. 8). The lowest maxima in concentrations at the deep mooring were 6- to 13-fold higher than the minimum during low tides 3, 5, 7, 8, and 9. During the second half of the series, the maxima were more stationary among tidal periods. Although they did not reach the degree observed during low tides 2 and 6, the maxima during tides 11 through 17 were between 28- and 54-fold higher than the series minimum. The anomalously high backscatter observed during high tide 15 is unexplained. We investigate the relationship between this among tidal-cycle variation in plankton concentration and variation in the physical environment (see 'Effect of physical variables on plankton' below).

When s_{rel} was examined as a function of the cumulative cross-isobath displacement of the tidal current, $d_{tide}(t)$, the concentration distribution of the zooplankton layer for the entire series became apparent in water mass space (Fig. 9). The concentration distribution in water mass space thus indicated that the moorings were located at a depth on the slope of the basin where they captured a horizontal boundary of the zooplankton layer, assuming that the mean position of the water mass during the series was at the mooring locations (0 km, Fig. 9). When the ADCPs sampled shallower water while the water mass was being displaced 1 to 5 km downslope ($-d_{tide}(t)$) from the deep mooring, s_{rel} consistently remained near the series minimum. It was only when the water was displaced beyond ~1 km downslope ($+d_{tide}(t)$) from the deep mooring that s_{rel} began increasing, indicating that the layer margin was located near the 120 m isobath during the mid-point of the tidal cycle.

Using the data illustrated in Fig. 9, we estimated the minimum cross-isobath width of the zooplankton layer, assuming that the mean position of the layer

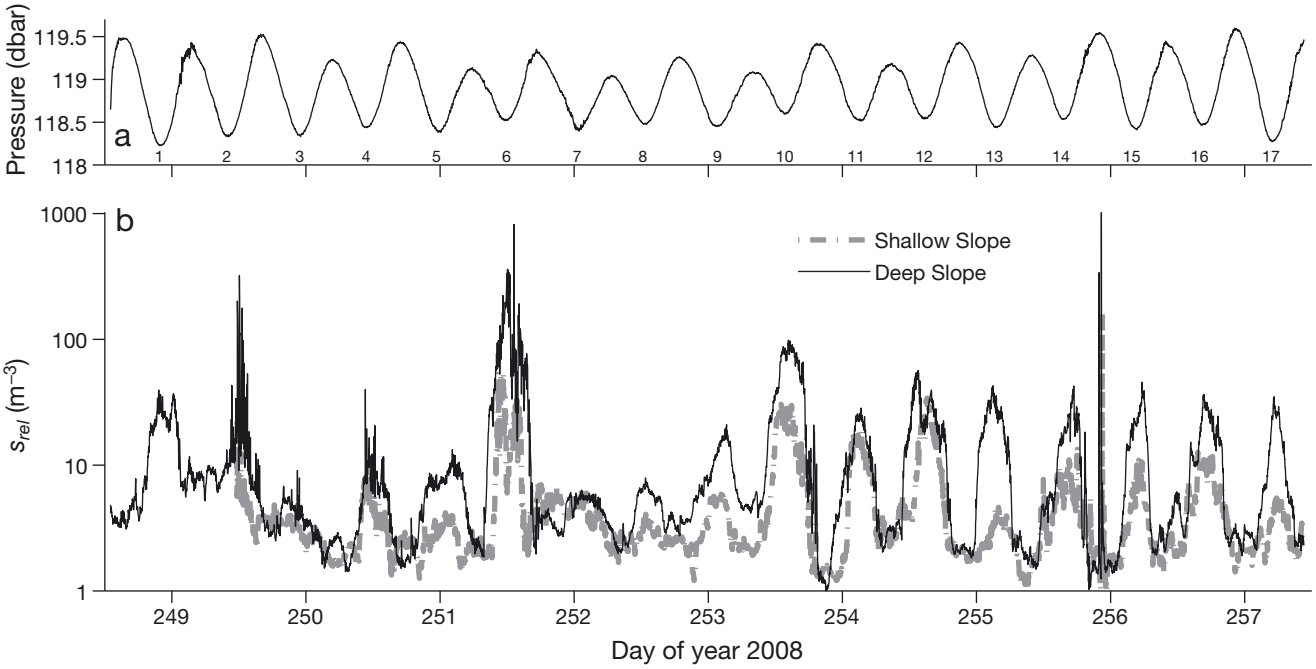

Fig. 8. Time series of (a) water pressure (dbar) at the deep-slope ADCP mooring in Roseway Basin, and (b) the layer-averaged relative zooplankton concentration (s_{rel} (t)) at the deep- (solid black line) and shallow-slope (grey dot-dash line) ADCP moorings. Tide sequence numbers (1–17) in (a) are referred to in the Results

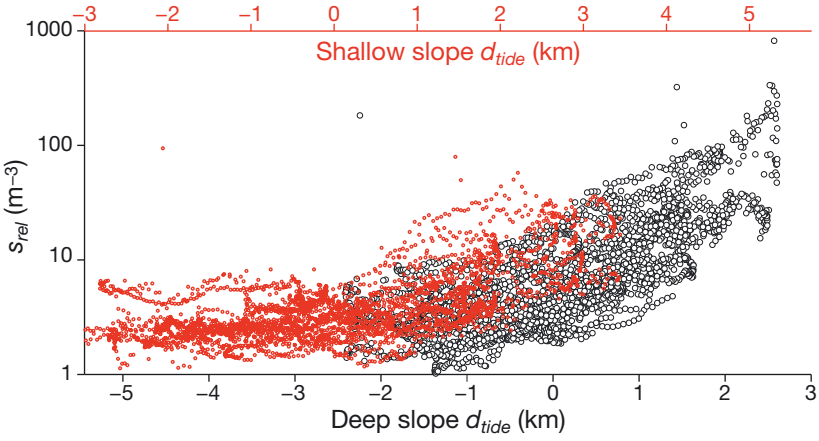

Fig. 9. Changes in layer-averaged relative zooplankton concentration ($s_{rel}(t)$) estimates (every second datum) in relation to upslope displacement or excursion (km) of water, $d_{tide}(t)$, at the deep-slope (black) and shallow-slope (red) ADCP moorings in Roseway Basin, where the upper and lower abscissas are shifted with respect to their cross-isobath separation distance of 2.7 km

boundary lay ~1 km downslope of the deep mooring (as above), and that when the layer washed upslope over the ADCPs, the instruments measured the closest zooplankton boundary but not the farthest boundary because it was presumably located more than 1 tidal excursion downslope of the deep mooring. This is a valid presumption because zooplankton concentrations clearly increased exponentially as the water moved upslope over the deep mooring during ebb tide, but did not plateau or decline again as the water moved farther upslope. Thus, we concluded that the minimum cross-isobath width of the layer was at least ~4 km, and likely greater because the exponential increase in s_{rel} only became readily apparent on the deep slope side of the water mass that we measured.

Effect of physical variables on plankton

Tidal advection

Each of σ_t, $d_{tide}(t)$, and s_{rel} consistently varied with the semi-diurnal tide at each mooring location (Figs. 3, 5 & 8), and the zooplankton were aggregated below the ~26 σ_t isopycnal that was advected with the tidal front. Thus, to further examine the variation in s_{rel} among tidal cycles, the log-transformed s_{rel} and σ_t anomalies were calculated and averaged over time between each maximum ebb and maximum flood tide (low tide-averaged), and the relations between the low tide-averaged s_{rel}, σ_t, and the maximum upslope extent of the tidal excursion (positive $d_{tide}(t)$) among low tides were examined using linear regression where the data from both moorings were aggregated. For the analyses involving the density anomaly, the 2 moorings were separated on the density axis by 0.06 kg m^{-3}; the average density difference measured between moorings during the second half of the series. Regression results indicated that ~60% ($p < 0.001$) of the variation in zooplankton concentration among tidal cycles was explained by variation in the upslope advection of zooplankton in a density gradient (Fig. 10). Therefore, processes that modulate the tidal excursion are a causal factor in zoopankton concentrations on the slope.

Low-density water mass origin

The origin of a low-density water mass that moved across the ADCP moorings during the first half of the series (water mass 2 in Fig. 4) and its associations with the current velocity is relevant because its presence co-occurred with the decrease in upslope tidal advection of plankton during most tidal cycles; compare, for example, the time series in Figs. 3a & 8. The low-density water mass may have been advected across the ADCPs in a cross-isobath direction and hence originated from on-bank. Two lines of evidence support this conclusion. Firstly, the cross-isobath residual constantly moved water in a downslope direction near the bottom (Fig. 6); this could advect lighter water downslope into the basin, thus explaining why the water on the slope gradually became less dense. Secondly, the water was less stratified between moorings during the first half of the series when the low-density water mass was present than in the second half when it was absent (Fig. 3a). If the tidal mixing front (Fig. 2a) was downslope of the ADCPs during the first half of the series, this would place the ADCPs on the well-mixed side of the front, and explain why there was little stratification between moorings during the first half of the series. When the low density front moved away from the ADCP locations, it did so by moving upslope toward the bank (Fig. 4). If the tidal mixing front also moved upslope at this time, the ADCPs would have been located on the stratified side of the front as was observed (Fig. 2a); this could explain why, during the second half of the series, the water was stratified between moorings (Fig. 3a). If the tidal mixing front

acted as a density barrier to upslope advection of plankton, its movement in a cross-isobath direction could have been responsible for the variation we observed in plankton concentrations on the slope.

Alternatively, water mass 2 may have been advected across the ADCP domain in an along-isobath direction by the subtidal flow, thus originating southwest of the ADCPs. Two pieces of evidence suggest an origin from the southwest along the isobaths. (1) Each of the large daily $d_V(t)$, and consequently the large-magnitude $d_{sub}(t)$ and the water mass were persistent during the first half of the series only. (2) The water mass moved off-shelf (Fig. 4) on the same day that the daily $d_V(t)$ began to decrease (Fig. 6). If the origin was along-isobath, then it is not possible to elucidate with this analysis whether mechanisms associated with the along-isobath velocity or with the low-density water mass damped the upslope tidal advection of plankton onto the slope, because the 2 were correlated — i.e. Would upslope advection have been damped if the along-isobath velocity was present without the low density water mass? Although our limited time series did not permit us to conclusively identify the origin of the low-density water mass, or its relationship with the current velocities, further research examining these alternative origin hypotheses will likely provide insights into the dynamics of the plankton–physics associations on the slope.

Along-isobath plankton distribution and advection

The along-isobath flow may also have caused variation in zooplankton concentration on the slope directly through along-isobath advection of the zooplankton layer. Assuming advection was the only mechanism affecting zooplankton concentration (i.e. no gains or losses within the layer), the along-isobath flow should provide insights into the distribution of zooplankton in the along-isobath direction. In the remainder of this sub-section, we explore the possibilities that zooplankton were associated with a particular water mass, or were randomly distributed or uniformly distributed along-isobath.

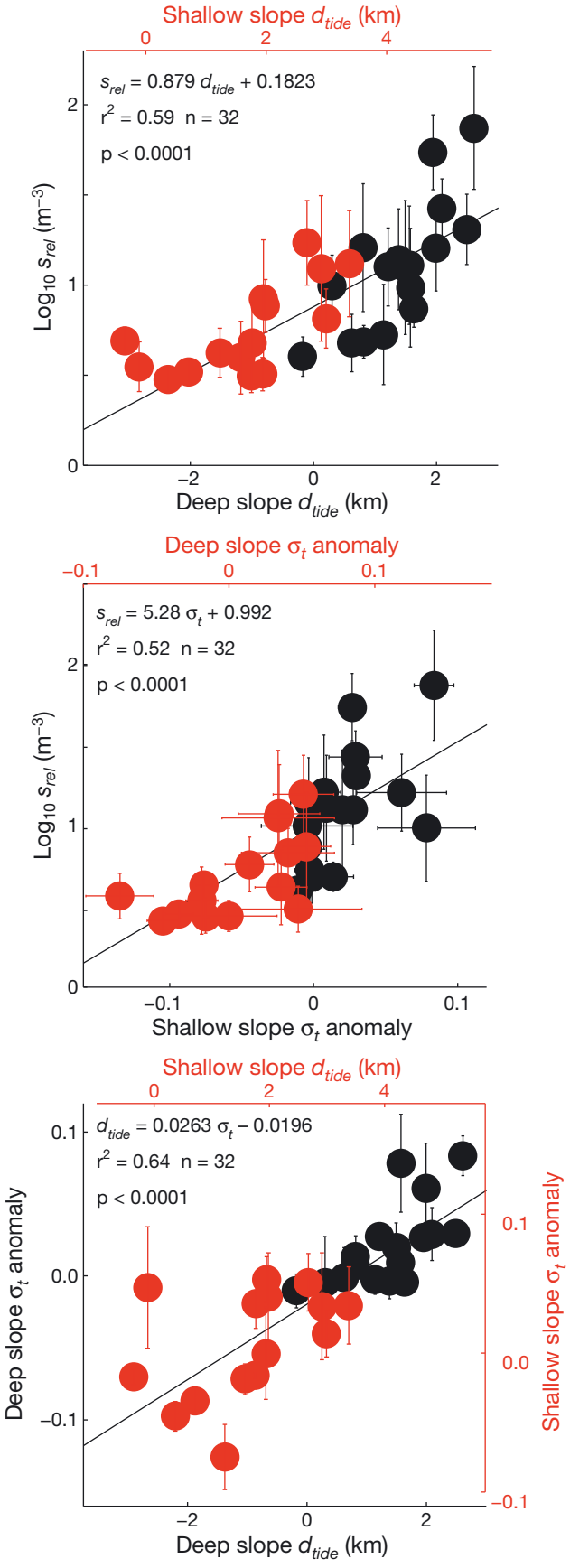

Fig. 10. Least-square regressions and associated statistics for each of the shallow- (red) and deep-slope (black) estimates, bounded by ±1 SD where possible, of (a) relative zooplankton concentration (s_{rel}) as a function of d_{tide}, (b) s_{rel} as a function of density (σ_t) anomalies, and (c) density (σ_t) anomalies as a function of d_{tide}. Mooring-specific data are separated by the 2.7 km distance between moorings or by the average 0.06 kg m^{-3} σ_t difference between moorings

If the zooplankton were associated with a particular water mass (e.g. $\sigma_t > 26$ kg m^{-3}) being advected along-isobath, we would expect zooplankton abundance to vary between the periods when the low-density water mass was present and when it was absent, assuming that the low-density water mass originated along-isobath to the southwest of the ADCPs. The decrease in density over the period when the low-density water mass was present spanned approximately the same range in density experienced between low and high tide when the low-density water mass was absent (~25.9 to 26.1 kg m^{-3}). Therefore, we expected to measure a decrease in zooplankton over the same time as the low-density water mass advected across the ADCPs, at least comparable in magnitude to that observed between high and low tide when the low-density water mass was absent; just over 1 order of magnitude change in zooplankton concentration. However, we found no clear association between zooplankton abundance and the low-density water mass, and no significant trend in zooplankton abundance was found in the first half of the series (Fig. 10, linear regression, $p > 0.1$ at both moorings). We concluded that hydrographic changes evolving from the low density water mass as it was advected along-isobath and across the ADCPs by the subtidal flow were not sufficient to explain variations in zooplankton concentrations on the slope.

If zooplankton were randomly distributed along-isobath in patches that were smaller than the length scale of the along-isobath flow, we expected to find no correlation between zooplankton abundance and the distance traveled upslope with the tide (maximum positive $d_{tide}(t)$) during the period when along-isobath advection was strong. This was not the case; the relationship between zooplankton concentration and the upslope extent of the tidal excursion was the same (and significant) regardless of the along-isobath flow being strong or weak. The simplest explanation, and consistent with our observations, was that the length scale of a fairly uniform (km scales; we do not address small-scale heterogeneity) zooplankton aggregation distributed along-isobath has a length scale greater than the along-isobath particle transport. In such a case, the along-isobath advection of the layer would not significantly change the concentration estimates at the ADCP locations over short time scales. The Eulerian $d_V(z,t)$ displacement measured at the ADCPs varied within the zooplankton layer with a scale of 40 (deep) to 90 (shallow) km over our deployment period (Fig. 7). Assuming a Lagrangian particle velocity of 2/3 the Eulerian velocity, which is valid for particles on a sloped boundary in a cross-isobath tidal velocity gradient (Loder 1980), the length scale of the layer in the along-isobath direction is 27 to 60 km. Roseway Basin is roughly 60 km in length along the southern margin, and the ADCPs were located at approximately 2/3 this length (40 km) from the western margin (Fig. 1). Thus, the southern margin to the west of the ADCPs is of insufficient length (~40 km) to accommodate a layer of zooplankton with the maximum length of ~60 km. This indicates some kind of copepod replenishment mechanism associated with the western margin of the basin.

It is entirely possible that our assumption of a 2D slab within which zooplankton concentrations did not appreciably change over time is invalid, although the average concentrations (Fig. 8) and displacement estimates above (Figs. 6 & 7) suggest otherwise. Nevertheless, we could, for example, consider that animals near bottom were retained along the southern margin longer than animals higher in the water column due to the depth-related shear in the subtidal flow (Fig. 7). We could also postulate one or more accumulating or dispersing mechanisms acting on the slope that served to maintain concentrations at a certain level regardless of concentration variation in the source water. Similar kinds of processes have been considered by others (e.g. Wishner et al. 2006, Aretxabaleta et al. 2008) and are explored below.

Zooplankton accumulation on the slope: a simple model

Zooplankton accumulation generated by a coupling of current velocities and zooplankton vertical velocities generated through sinking, floating, or directed swimming, has been demonstrated by modeling studies (e.g. Franks 1992). Thus we can ask whether it is possible that patches of diapausing copepods were accumulated through a combination of the current velocity and the copepods maintaining their vertical position. Assuming that the diapausing copepods were neutrally buoyant in water of a given density to which they had become physiologically acclimatized (i.e. they have achieved neutral buoyancy), then it is reasonable to conclude that if they were advected above or below this density, they would maintain their vertical position (in density space) by sinking or floating back to their depth of neutral buoyancy. To examine this proposed accumulation mechanism on the sloped margin of Roseway Basin, we extended our 2D analyses above to include the vertical and horizontal structure in the current velocity estimates. Our goal was to determine the effects of sheared

dU/dx and dU/dz on plankton concentrations within the layer. Having the 2 ADCP moorings deployed cross-isobath, and within 1 tidal excursion (i.e. they overlapped in water mass space), allowed us to infer flow-fields within the domain between the moorings at each time step of our deployment and thus to examine the horizontal structure of currents in the cross-isobath dimension (dU/dx). Vertical structure (dU/dz) was included based on each of the ADCP horizontal current measurements at a 1 m depth resolution (z-layers) throughout the water column.

As a first step, we developed a simple 1D flow-field model using our measured cross-isobath velocities ($U(x,z,t)$, where x = cross-isobath position, z = depth, t = time). The equations of continuity cannot be satisfied with this simple model, and our purpose was to identify fundamental processes and then develop hypotheses for subsequent testing using more advanced models. First, we linearly interpolated U (m s^{-1}) between the 2 moorings at each z-layer (1 m) between 50 m and the bottom at every 2 min time step. We restricted the model domain to below 50 m because (1) copepods were not aggregated at the shallow depths, and (2) current estimates in the shallows (farther from the transducers) had large uncertainties. Our moorings were located on a slope, and bathymetric steering of the currents near bottom meant that interpolating between the same depths at both moorings was not appropriate for all depths, particularly those near bottom. Therefore, depth pairs between moorings were selected by assessing correlations in current velocity at all time steps between each possible depth pair. Pairs that were well correlated (highest r^2) were then selected and used in the interpolation. The interpolation resulted in a matrix of cross-isobath velocities at each time step for each z-layer and 100 m horizontal spacing in the cross-slope direction.

We initialized the flow-field model with particles uniformly distributed across the z-layers using a 100 m cross-isobath (x) resolution (Fig. 11), similar to Franks (1992), and we ran the particle tracking model for a full tidal cycle between 2 adjacent maximum ebb tides. Particles that left the domain were problematic as we had no current information external to the domain. To minimize the problem, we proceeded as follows: (1) only the deep-slope half of the model domain was seeded with particles, consistent with the observations, (2) the period for a model run was restricted to 1 tidal cycle because a large proportion of the particles would leave the domain and not return over longer periods due to the cross-isobath subtidal flow, (3) maximum ebb tides were chosen as time boundaries, although alternatively, the time period between adjacent maximum flood tides would have achieved the same result if the shallow-slope half of the model was seeded with particles, and (4) if particles left the model domain at the deeper or shallower boundaries, they were assumed to advect at the same speed they experienced at the model boundary. Particles were prevented from moving along the sloped bottom, and density stratification was not considered. The model was run over each tidal cycle throughout the 9 d current-data series.

The results of the modeling are based on 3 different tidal cycles (see Fig. 3 that illustrates oceanographic conditions and tide-sequence numbering) that represented a range of physical oceanographic conditions observed in the along-isobath subtidal flow (Fig. 11): (1) cycle 3; a period of strong along-isobath current, (2) cycle 10; a period when the along-isobath current began to slow near neap tide, and (3) cycle 17; a period of near-zero along-isobath current below 100 m. On the completion of each model run, we calculated the depth averaged particle-to-particle horizontal distance (an estimate of dU/dx since the particles are initiated with equal spacing) for each of the ebb- and flood-tide phases to quantify zones of apparent particle compression or decompression relative to the initial state (as defined by Franks 1992). Because the 1D model precludes continuity equations, the terms compression and decompression describe only the change in particle-to-particle distance; i.e. apparent compression ≠ particle accumulation and apparent decompression ≠ particle dispersal. Putting the compression and decompression zones into a more formal context requires a more sophisticated 3D model and analysis.

Despite the simplicity of the 1D model, some interesting and recurrent patterns in the cross-isobath particle distribution were apparent. During the initial upslope (ebbing) tidal phase, a small compression or small decompression among particles was apparent, but as low tide approached, more decompression occurred (Fig. 11, Hour-3). During the downslope (flooding) tidal phase, the particles were always compressed and compression tended to increase near bottom (Fig. 11, Hour-6 and Hour-9). When the along-isobath current was strong, the upslope tidal phase (ebbing) was also, on average, in a compressive state. When the along-isobath current was absent, 3 of the 8 tidal cycles showed decompression on the upslope ebbing phase (Fig. 11, Tide 17), and the remainder showed a small overall compression on the upslope phase. Finally, when decompression occurred on the upslope phase, it was always less

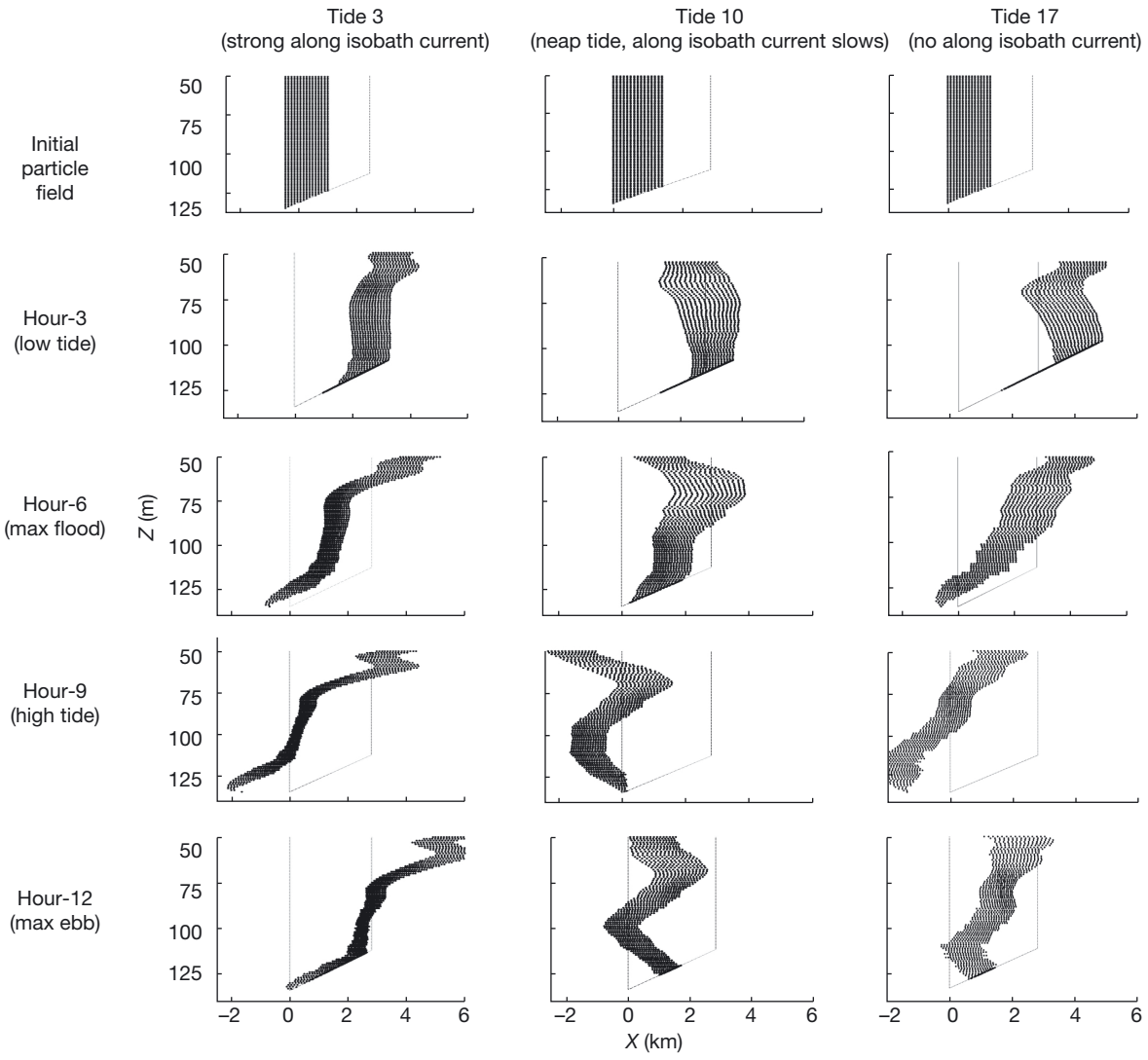

Fig. 11. Particle-tracking model results for 3 tidal cycles (tide sequence numbers shown in Figs. 4 & 9) representing periods of strong along-isobath current (Tide 3, left panels), slowing along-isobath current at neap tide (Tide 10, middle panels) and no along-isobath current (Tide 17, right panels), where the evolution of particle compression and decompression is illustrated from initialization at near maximum ebb tide through 3 h increments of the tidal cycle to near maximum flood tide. The abscissa, *X*, represents the cross-isobath displacement distance with respect to the deep-slope ADCP and the ordinate, *Z*, is depth (m) below surface. The model domain is outlined with a grey line that reflects the sloping bottom that was linearly interpolated between the seafloor depths at each ADCP location

than the compression apparent on the preceding downslope phase. Taken together, these results show that particles will compress in a cross-isobath direction, creating a convergence zone for water on the slope that is maintained through time.

Compression or decompression occurs because of cross-isobath gradients in the cross-isobath currents (i.e. dU/dx). Compression on the downslope phase of the tide can easily be explained by the gradient in tidal currents between moorings (Fig. 5). Faster-moving water at the shallow mooring, pushing on slower water deeper in the basin, will create an apparent compression. The absence of an equal and opposite decompression on the upslope phase that should result from the same gradient, however, is more difficult to explain. One part of the explanation comes from the cross-isobath component of the subtidal flow, which below 80 m depth is always directed downslope regardless of tidal phase (Fig. 7). This flow is greater in velocity at the shallow mooring than at the deep mooring and works against the decompressive gradient on the upslope tidal phase. This flow also explains why compression is greatest near bottom, where the cross-isobath subtidal flow is strongest (Fig. 7).

When the along-isobath component of the subtidal flow was present, a compressive 'sweet spot' occurred

in the 75 to 120 m (Tide 3 in Fig. 11) depth layer that encompassed the depths of highest concentrations of copepods (Fig. S1). Below 120 m, particles tended to be swept downslope by the cross-isobath component of the subtidal flow (Fig. 7). Above 75 m, they were swept toward the open ocean as the subtidal flow veers seaward in the upper Ekman layer (Fig. 7). Within the 75–120 m layer, we observed little to no vertical shear in the cross-isobath currents, and this would serve to help maintain the vertical integrity of advecting zooplankton patches as they are displaced along the slope. This simple mechanism could help maintain (and possibly accumulate; see Discussion) high concentrations of diapausing copepods on the slope.

DISCUSSION

We have shown that copepods diapausing at depth in the southern slope margin of Roseway Basin were advected by a cross-isobath tidal current that converged on the slope, where the animals were advected along-isobath by a subtidal mean flow near a tidal mixing front. The animals were generally evenly distributed in an along-isobath direction, and new individuals advecting along-isobath with the mean flow appeared not to be retained along the slope for more than a few days. Our simple particle model illustrated that gradients in the cross-isobath currents also appear to play a role in maintaining and possibly accumulating the diapausing copepods on the southern slope margin. Our Eulerian description of the habitat provided valuable insights, but adequate characterization of the mechanisms affecting the right whale prey field required the additional Lagrangian description of the biological and physical environment that was provided by the particle model. Below, we develop hypotheses concerning sources and retention mechanisms for copepods in the basin, and discuss the results of our simple accumulation model, suggesting how it can be extended in the future to provide even greater insights.

The Eulerian velocity on the southern slope of the basin was equivalent to a displacement distance of 10 to 15 km d^{-1}, and, assuming the Lagrangian particle velocity is 2/3 of the Eulerian velocity (Loder 1980), individual copepods are unlikely to be retained along the 60 km long slope for more than ~7 d when an along-isobath current is present. Tidally rectified flow around nearby Browns Bank occurs year-round with no strong seasonal pattern and varies primarily in response to tidal forcing (Smith 1989). Density-driven flow also occurs to some degree throughout the year (Loder et al. 1997, Hannah et al. 2001). Thus, as suggested above, a mechanism must exist near the western end of the basin that provides continuous replenishment of the high concentrations of copepods that are swept along-isobath by the subtidal flow on the southern slope. The 3 most likely mechanisms for copepod replenishment to the deeper waters on the southeastern slope are not mutually exclusive: a continuous surface supply, recirculation within the basin, and continuous along-isobath through-flow.

Continuous surface supply

If there is a surface supply, the copepod population at depth can be replenished vertically as new individuals in the surface layer enter diapause and sink below ~75 m depth. These individuals most likely originate upstream either in the Gulf of St. Lawrence, from populations associated with other shelf basins on the eastern Scotian Shelf, or slope waters intruding onto the shelf in spring (Herman et al. 1991, Head et al. 1999). These 'source' populations could be advected to the western basins, including Roseway, by shelf circulation. The paucity of appreciably high concentrations of copepods in the surface layers on the shelf suggests that this supply, measured as point estimates, is diffuse in time and space and cannot alone account for the large concentrations found at depth and along the southeastern slope (Herman et al. 1991).

Basin recirculation

Seasonal models for the basin describe a gyre-like circulation created by the along-isobath subtidal flow maintained partially by rectification and density-driven effects (Hannah et al. 2001). Thus, in relation to a basin recirculation mechanism, diapausing copepods sinking to depth from the surface, or horizontally advected into the basin, may become trapped below the basin sill and advected continuously around the basin by the gyre. Our data, and those presented by Smith (1989), are consistent with the presence of gyre-like circulation within the basin. Copepods in nearby Emerald and Lahave Basins are aggregated with a generally uniform kilometer-scale distribution at depth, and surface supply, coupled with an at-depth circulation that is postulated to maintain the aggregations (Herman et al. 1991). A gyre, however,

is not in itself sufficient to explain why right whales in Roseway Basin predominantly forage along the southern margin of the basin. Although not addressed by Herman et al. (1991), their data also illustrate elevated copepod concentrations on the southern slopes of both the Emerald and Lahave Basins at depths of between 150 and 200 m that are shallower than the mid-basin concentrations. Slope aggregations of this type are likely overlooked, as they are small features relative to the mid-basin aggregations. As suggested above, gyre-like recirculation, coupled with a copepod-accumulating mechanism acting on the slope, could explain such distributions in the other nearby shelf basins.

The depth distributions of slope aggregations relative to the deep basin aggregations may make the former more beneficial to feeding whales despite the slope region being relatively small in area and hence a smaller but more concentrated prey-field. Such a benefit may be related to a depth limit below which the energy gained by the whales feeding at greater depth does not outweigh energy expended by diving to greater depth, thus limiting foraging to the relatively shallow (<120 m) regions of high concentrations of copepods. Such a limitation may explain why right whales are rarely observed in the deeper Emerald and Lahave Basins, despite appearing as potential habitat containing high concentrations of copepods. We caution, however, that right whale occupancy estimates for these other basins are essentially non-existent, although there is some evidence that right whales occasionally occupy Emerald Basin (Mellinger et al. 2007).

The dynamic forcing of the cross-isobath subtidal flow (U_{sub}) is particularly relevant to the above recirculation interpretation because it, along with the cross-isobath tide, contributes to the generation of an apparent compression zone as defined by Franks (1992) for copepod-filled waters on the slope. That the cross-isobath component of the subtidal flow did not slow near-bottom after neap tide with the along-isobath flow, and remained relatively stable throughout our monitoring period, indicates that at subtidal frequencies the along-isobath and cross-isobath flows were not dynamically related. The cross-isobath residual was also not a local or ephemeral event as our observations are consistent with those of Smith (1989) for the northern flank of nearby Browns Bank. The cross-isobath flow is thought to originate from buoyancy fluxes associated with the barotropic and baroclinic tidal interactions on a slope (Ou & Maas 1986), meaning that this flow should be stronger in steeper areas than in areas with a weaker bathymetric gradient. If it is a general mechanism on sloped boundaries on the shelf, such a flow could help generate convergence zones for zooplankton on other steep slopes on the shelf, including in Lahave and Emerald Basins.

It is also possible that the slope is an actual compression zone, which is a type of accumulation zone (Franks 1992). The vertical currents measured by the ADCPs at the deep mooring were either consistently directed toward the surface (assuming the RDI data were reliable) or consistently directed downward (assuming the Aquadopp data were reliable) throughout the time series. Copepods compressing on the slope and advected upward or downward must sink, float, or swim to maintain their vertical position at depth, or else be advected out of the basin in the upper water column or sink to the bottom. We postulate that cross-isobath compression, coupled with vertical position maintenance, could act to accumulate copepods at depth on the sloped margin. The relative stationarity of the density field within the basin over time in response to larger fluctuations in water mass temperature and salinity on both short (Fig. 3, second half of series), and long time scales (Smith 1989), may be beneficial to diapausing copepods because the maintenance of their position in the water column depends on water column density. A similar cross-isobath compression and vertical position maintenance mechanism was proposed for copepods on the northern flank of Georges Bank by Wishner et al. (2006) and in the Grand Manan Basin by Michaud & Taggart (2007) and may be a general mechanism acting on sloped boundaries with cross-isobath tidal ellipses. Testing this hypothesis will require mapping the cross-isobath density field using a time series of CTD sections, modeling copepod buoyancy in relation to the density field, and extending the flow field model to 3 dimensions with continuity and conservation compliance as achieved by Aretxabaleta et al. (2008).

Assuming that a gyre-like structure does exist in Roseway Basin, we have no evidence that it is closed. Our data demonstrated that density-driven flow does occur on both the northeastern and southeastern margins of the basin where the isopycnals are tilted in a cross-isobath direction. This would help maintain a gyre, but density-driven flow needs to be confirmed for the eastern and western margins. Although we did identify the oceanographic conditions necessary for local tidal rectification, basin-scale rectification is unlikely as the tidal excursions become very small at the eastern margin of the basin, the bathymetric gradients are small along the eastern and western margins, and the deep channels at either end of the basin interrupt the sloping bathymetry (Fig. 1). As a consequence,

deep water inflow and outflow between Roseway Basin and other shelf or slope waters may transport copepods into or out of the basin.

Continuous along-isobath through-flow

Copepods concentrated at depth along the southern margin of the basin may be replenished by an along-isobath flow entering the basin from the western margin between the deep channel separating Browns Bank and Nova Scotia and flowing along the southeastern slope to exit the basin at the eastern margin via the channel separating Baccaro and Roseway Banks (Fig. 1a). Smith (1989) measured inflow to Roseway Basin on the northern flank of Browns Bank that was generated by rectification around the bank. Eastward flow, at depth, in the Browns Bank–Nova Scotia channel in summer is postulated as being dynamically related to deep inflow from the Northeast Channel (Hannah et al. 2001), and thus, one copepod source may be populations overwintering on the Scotian Slope that enter the shelf region and Roseway Basin via the Northeast Channel.

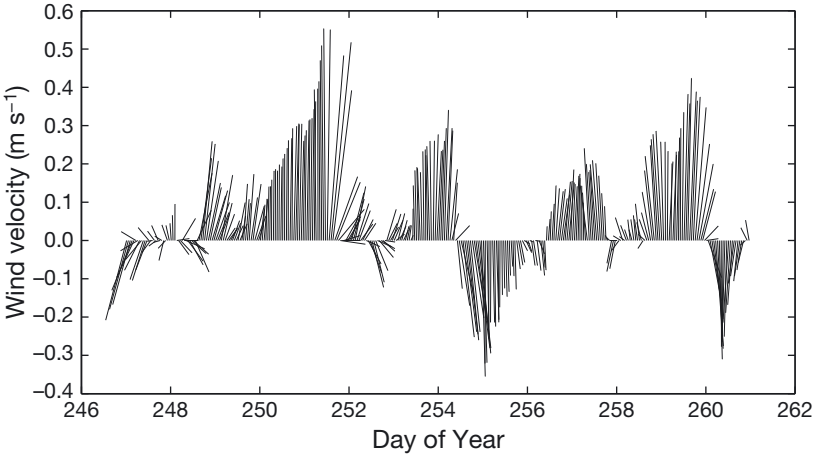

Fig. 12. Wind-stick compass representation of hourly wind velocity (m s^{-1}; N is +ve, vertical) collected at the Environment Canada weather buoy LaHave Bank 44150 (42.5°N, 64.02°W) near the ADCP mooring locations during Days 247 through 261, 2008. The wind direction is the direction toward which the wind is blowing, for comparison with the oceanographic data

We determined that the along-isobath flow could be forced by baroclinicity and tidal rectification. Along-isobath flow could also be generated through wind forcing at the surface, although this far-field forcing is expected to have a more immediate impact on surface waters, and our sampling location is at ~100 m depth. It is possible that changes in the local wind patterns, hours or days beforehand, could have affected the current velocities we observed at the ADCP locations. We examined hourly wind magnitude and direction data collected at the nearest marine weather buoy (Environment Canada, LaHave Bank 44150, 42.5°N, 64.02°W; www.weatheroffice.gc.ca/marine/weatherConditions-currentConditions_e.html?mapID=15&siteID=14100&stationID=44150) between 3 and 16 September 2008 (Days 247–260 inclusive; Fig. 12). These data showed the dominant wind direction was toward the north from Day 248 to 251, and was particularly strong in magnitude reaching 0.5 m s^{-1} on Day 251. During this period, the along-isobath velocity at the ADCP moorings was strong, and therefore may have been partially generated by surface winds. Around midnight on Day 252, the wind abruptly declined in magnitude and blew toward the south, and at approximately the same time that the along-isobath flow declined in magnitude (Fig. 6). Thereafter, the wind blew toward the north for 2 d, then toward the south for 2 d, often reaching similar magnitudes as before Day 252, and during this time, no along-isobath flow was measured at the ADCP moorings. A more rigorous analysis was not performed because of the far-field nature of the wind forcing. However, we can tentatively conclude that, along with tidal rectification and the density structure, wind forcing is a potential, but not definitive, driver of along-isobath subtidal flows along the southern slope of Roseway Basin.

In summary, we found that diapausing copepod aggregations on the southern slope of Roseway Basin are advected cross-isobath with the tide. Individual copepods do not appear to remain on the slope for long because they are advected along-isobath by the mean flow. That fact that high copepod concentrations are maintained on the southern slope, despite along-isobath emigration, implies that there must be one or more replenishing and concentrating mechanisms. We postulate that these mechanisms include vertical and/or horizontal immigration to the deep basin and gyre-like re-circulation within the basin. We provided evidence that shear in the horizontal currents, coupled with buoyancy-related maintenance of vertical position, could act in concert to accumulate copepods along the southern slope region of the basin. The accumulation of the copepods makes the slope region a beneficial feeding ground for right whales relative to the rest of the basin, and thus explains why the highest probability of sighting a right whale occurs along the southern slope and not elsewhere.

Acknowledgements. We thank D. Brownell, M. Hatcher, W. Judge, D. Schillinger, R.K. Smedbol, A. Vanderlaan, and the crew of the RV 'Dominion Victory' for help with field work; M. Morgan, J. Slade, and A. Ryan for sample processing; and A. Hay, B. deYoung, and Defense Research and Development Canada for providing equipment. We thank B. Petrie, Y. Simard, and K. Thompson for insights and suggestions, and 3 referees who generously contributed to and improved the manuscript. Funding for this research was provided to C.T.T. by the Fisheries and Oceans Canada Species at Risk Program, the Environment Canada - WWF Endangered Species Fund, the Environment Canada Habitat Stewardship Program, and a Natural Sciences and Engineering Research Council (NSERC) Discovery Grant. K.T.A.D. was supported by an NSERC PSG-M Scholarship.

LITERATURE CITED

Aretxabaleta AL, McGillicuddy DJ Jr, Smith KW, Lynch DR (2008) Model simulations of the Bay of Fundy gyre. 1. Climatological results. J Geophys Res 113:C10027, doi: 10.1029/2007JC004480

Baumgartner MF, Cole TVN, Clapham PJ, Mate BR (2003) North Atlantic right whale habitat in the lower Bay of Fundy and on the SW Scotian Shelf during 1999–2001. Mar Ecol Prog Ser 264:137–154

Campbell RW (2008) Overwintering habitat of *Calanus finmarchicus* in the North Atlantic inferred from autonomous profiling floats. Deep-Sea Res I 55:630–645

Campbell RW, Dower JF (2003) Role of lipids in the maintenance of neutral buoyancy by zooplankton. Mar Ecol Prog Ser 263:93–99

Davies KTA, Ryan A, Taggart CT (2012) Measured and inferred gross energy content in diapausing *Calanus* spp. in a Scotian Shelf basin. J Plankton Res 34:614–625

Deines KL (1999) Backscatter estimation using broadband Acoustic Doppler Current Profilers. In: Proceedings of the IEEE 6th working conference on current measurement, 1999, p 249–253

Franks PJS (1992) Sink or swim: accumulation of biomass at fronts. Mar Ecol Prog Ser 82:1–12

Hannah CG, Shore JA, Loder JW, Naimie CE (2001) Seasonal circulation on the western and central Scotian Shelf. J Phys Oceanogr 31:591–615

Head EJH, Harris LR, Petrie B (1999) Distribution of *Calanus* spp. on and around the Nova Scotia shelf in April: evidence for an offshore source of *Calanus finmarchicus* to the central and western regions. Can J Fish Aquat Sci 56: 2463–2476

Herman AW (1988) Simultaneous measurement of zooplankton and light attenuance with a new optical plankton counter. Cont Shelf Res 8:205–221

Herman AW (1992) Design and calibration of a new optical plankton counter capable of sizing small zooplankton. Deep-Sea Res A 39:395–415

Herman AW, Sameoto DD, Shunian C, Mitchell MR, Petrie B, Cochrane N (1991) Sources of zooplankton on the Nova Scotia shelf and their aggregation within deep basins. Cont Shelf Res 11:211–238

Kraus SD, Rolland RM (2007) Right whales in the urban ocean. In: Kraus SD, Rolland R (eds) The urban whale: North Atlantic right whales at the crossroads. Harvard University Press, Cambridge, MA, p 1–38

Laurinolli MH (2002) Localisation of North Atlantic right whale (*Eubalaena glacialis*) sounds using hydrophone arrays in the Bay of Fundy. MSc dissertation, Dalhousie University, Halifax, NS

Loder JW (1980) Topographic rectification of tidal currents on the sides of Georges Bank. J Phys Oceanogr 10: 1399–1416

Loder JW, Han G, Hannah CG, Greenberg DA, Smith PC (1997) Hydrography and baroclinic circulation in the Scotian Shelf region: winter versus summer. Can J Fish Aquat Sci 54:40–56

Mellinger DK, Nieukirk SL, Matsumoto H, Heimlich SL and others (2007) Seasonal occurrence of North Atlantic right whale (*Eubalaena glacialis*) vocalizations at two sites on the Scotian Shelf. Mar Mamm Sci 23:856–867

Michaud J, Taggart CT (2007) Lipid and gross energy content of North Atlantic right whale food, *Calanus finmarchicus*, in the Bay of Fundy. Endang Species Res 3: 77–94

Michaud J, Taggart CT (2011) Spatial variation in right whale food, *Calanus finmarchicus*, in the Bay of Fundy. Endang Species Res 15:179–194

Ou HW, Maas L (1986) Tidal-induced buoyancy flux and mean transverse circulation. Cont Shelf Res 5:611–628

Pawlowicz R, Beardsley B, Lentz S (2002) Classical tidal harmonic analysis including error estimates in MATLAB using T_TIDE. Comput Geosci 28:929–937

Sameoto DD, Jaroszynski LO, Fraser WB (1980) BIONESS, a new design in multiple net zooplankton samplers. Can J Fish Aquat Sci 37:722–724

Sartoris FJ, Thomas DN, Cornils A, Schnack-Schiel SB (2010) Buoyancy and diapause in Antarctic copepods: the role of ammonium accumulation. Limnol Oceanogr 55:1860–1864

Schaeff CM, Krauss SD, Brown MW, White BN (1993) Assessment of the population structure of western North Atlantic right whales (*Eubalaena glacialis*) based on sighting and mtDNA. Can J Zool 71:339–345

Smith P (1989) Circulation and dispersion on Browns Bank. Can J Fish Aquat Sci 46:539–559

Taylor JR, Sarkar S (2008) Stratification effects in a bottom boundary layer. J Phys Oceanogr 38:2535–2555

Vanderlaan ASM, Taggart CT (2009) Efficacy of a voluntary area to be avoided to reduce risk of lethal vessel strikes to endangered whales. Conserv Biol 23:1467–1474

Vanderlaan ASM, Taggart CT, Serdynska AR, Kenney RD, Brown MW (2008) Reducing the risk of lethal encounters: vessels and right whales in the Bay of Fundy and on the Scotian Shelf. Endang Species Res 4:283–297

Vanderlaan ASM, Taggart CT, Smedbol RK (2011) Fishing-gear threat to right whales (*Eubalaena glacialis*) in Canadian waters and the risk of lethal entanglement. Can J Fish Aquat Sci 68:2174–2193

Visser AW, Jonasdottir SH (1999) Lipids, buoyancy and the seasonal vertical migration of *Calanus finmarchicus*. Fish Oceanogr 8:100–106

Wishner KF, Outram DM, Ullman DS (2006) Zooplankton distributions and transport across the northeastern tidal front of Georges Bank. Deep-Sea Res II 53:2570–2596

Woodley TH, Gaskin DE (1996) Environmental characteristics of North Atlantic right and fin whale habitat in the lower Bay of Fundy, Canada. Can J Zool 74:75–84

Editorial responsibility: Alejandro Gallego, Aberdeen, UK

Submitted: March 5, 2012; Accepted: November 21, 2012
Proofs received from author(s): March 6, 2013